

Preparation and improved energy storage capability of nanocomposites utilizing ultrathin 2D HfO₂@TiO₂ nanosheets

Chao Chen^{†,‡,¶}, Chen Guo^{†,*}, Xiaoyong Wei[†] and Pengfei Wang^{†,§,¶}

^{*}Xi'an Institute of Optics and Precision Mechanics

Chinese Academy of Sciences (CAS), Xi'an 710119, China

[†]Electronic Materials Research Laboratory, Key Laboratory of the Ministry of Education and International Center for Dielectric Research, Xi'an Jiaotong University

Xi'an 710049, China

[‡]chenchao@opt.ac.cn

[§]pfwang@opt.ac.cn

Received 11 September 2023; Revised 23 October 2023; Accepted 24 October 2023; Published 15 November 2023

Polymer-based dielectrics play an important role in electrostatic capacitor by their high energy density (U_e) and flexibility. Herein, we designed a simple high U_e polymer-based dielectrics by controlling the morphology and surface modification of inorganic fillers. To decrease the difference in dielectric properties between fillers and matrix of the nanocomposites, HfO₂ acting as the buffer layer with high insulation and appropriate permittivity coated onto the surface of TiO₂ nanosheets (TiO₂ Ns) to form a core-shell structure. The introduction of HfO₂@TiO₂ nanosheets (HfO₂@TiO₂ Ns) makes the nanocomposite with higher dielectric permittivity and lower dielectric loss than poly(vinylidene fluoride-co-hexafluoropropylene) (P(VDF-HFP)) matrix. In addition, the HfO₂@TiO₂ Ns can establish an efficient barrier to limit the space charge conduction, hamper the growing electric trees, and the HfO₂ layer with high insulation could hinder the mobility of charge carriers. The breakdown strength (E_b) of nanocomposite is superior to that of polymer matrix. A small addition of 3 wt.% HfO₂@TiO₂ Ns into P(VDF-HFP) matrix can raise the E_b to 480.7 MV/m and present a maximum discharged U_e of 13.9 J/cm³. This work demonstrates that it is an effective strategy to improve the U_e via designing the structure and surface state of inorganic filler simultaneously.

Keywords: Nanosheets; nanocomposite dielectrics; passivation layer; breakdown strength; energy density.

1. Introduction

With the increasing demand for energy in modern society, renewable energies such as wind, hydro, solar and nuclear resources have attracted more and more attention and research. In order to maximize the utilization of these energy resources, reliable and efficient energy storage equipment appears especially essential.¹⁻³ Polymer-based dielectrics have been investigated and utilized in commercials by reason of ultrahigh power density, fast charge-discharge rate and flexibility, such as in pulsed power generators, rail guns, lasers, and electromagnetic launch systems.^{4,5} However, the low U_e critically hinders the application of polymer dielectrics in electronics field. Therefore, it is necessary to improve its U_e to meet the practical application requirements.^{6,7}

In practical applications, the electric displacement (D) and discharged U_e of the dielectric capacitors can be calculated by the following formulas⁸:

$$D = \varepsilon_0 \varepsilon_r E, \quad (1)$$

$$U_e = \int_{D_r}^{D_{\max}} E dD, \quad (2)$$

where ε_0 , ε_r , E , D_{\max} , D_r are the permittivity of vacuum, relative permittivity, electric field, maximum electric displacement, and remnant electric displacement. It can be seen that U_e is closely associated with the ε_r and E . Therefore, high- ε_r ceramic fillers, such as BaSrTiO₃(BST) and CaCu₃Ti₄O₁₂(CCTO), were usually added into polymer to improve the ε_r .⁹⁻¹²

The ε_r of composites is equal to the integral $\varepsilon_r = f_1 \varepsilon_1^a + f_2 \varepsilon_2^a$, where ε_1 , ε_2 , f_1 and f_2 are the ε_r of polymer, ε_r of fillers, volume fraction of polymer and fillers, respectively.¹³ It is generally necessary to introduce a lot of inorganic ceramics to realize the obvious increase of dielectric permittivity of polymer-based nanocomposites. Nevertheless, nanofillers can agglomerate with high surface energy, causing poor dispersity in matrix.¹⁴ Moreover, the addition of large amount of ceramic fillers may lead to field distortion and structural defects, which is unfavorable to improving

[¶]Corresponding authors.

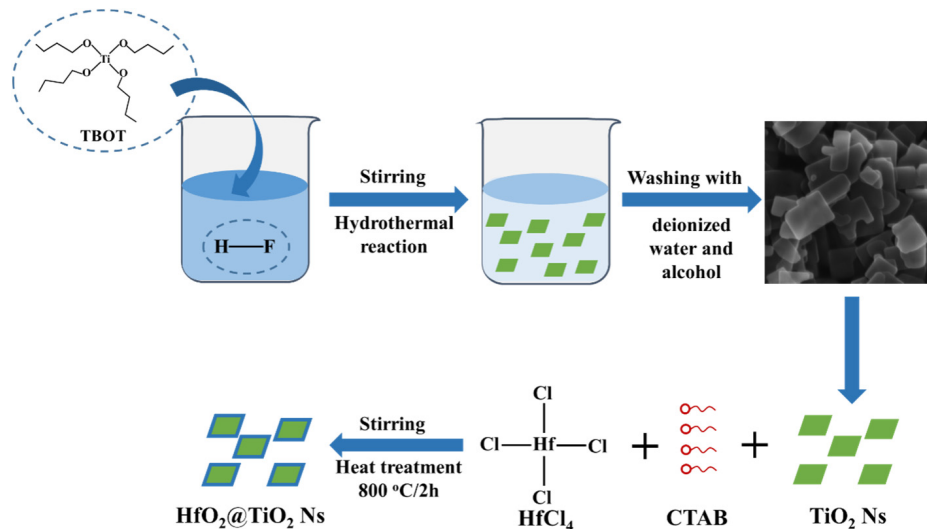
U_e . To improve the dispersion of ceramics and the difference of electrical properties between polymer and ceramic in nanocomposites, such as ceramic surface ionization, surface grafting, organic coating and inorganic coating could be used as a way of surface treatment.^{15–19} For example, the Huang research group has reported an effective way to prepare poly (methyl methacrylate) (PMMA)-based nanocomposites.²⁰ In these nanocomposites, the PMMA@BT was dispersed in matrix, and the PMMA@BT nanocomposites showed a significantly increased ϵ_r and lower dielectric loss compared with pristine PMMA. Zhai prepared a core-shell structured Al_2O_3 @BT ferroelectric nanoparticle, amorphous Al_2O_3 layer with wide band gap that can effectively inhibit the leakage current and field distortion, thereby enhancing the U_e .²¹

Recently, it has been shown that nanostructures and filler loads have a significant impact on the U_e of nanocomposites.²² Compared with nanoparticles, 2D nanosheets can more greatly enhance the U_e at low content of inorganic fillers.^{15,23} The reason is that the nanosheets with large aspect ratio can build a charge barrier in the nanocomposite, which limits the growth of the breakdown path. Therefore, the 2D nanosheets can enhance the U_e of nanocomposites.^{4,15}

TiO_2 can be widely used as an inorganic filler of polymer-based nanocomposites because of its excellent corrosion resistance, thermal stability and biocompatibility.^{24,25} In addition, the preparation method of TiO_2 is very simple, and the reaction conditions and growth rate of different crystal planes can be controlled by extremely simple methods. The final TiO_2 products with different morphologies and dimensions were obtained, mainly including hollow microspheres, nanosheets, nanowires, morphology, etc.^{26–29} As a widely used inorganic material, titanium dioxide (TiO_2) has wide band gap and high ϵ_r . For instance, Ki-Seok introduced

2D TiO_2 nanosheets (TiO_2 Ns) into the PVA matrix and the nanocomposite reaches a high ϵ_r of 43.8.³⁰ Wong selected the 2D TiO_2 Ns as the electron scattering source to enhance the U_e of the nanocomposite, which possesses the largest E_b of 561.2 MV/m.³¹ Introducing dopamine-modified TiO_2 (TiO_2 @PDA) nanosheets into the PVDF matrix, 9 wt.% TiO_2 @PDA/PVDF with a superior U_e of 10.53 J/cm³, which is 1.75 times of pristine PVDF (6.01 J/cm³).²⁵ Therefore, TiO_2 Ns is a kind of convenient and effective inorganic filler, which can be used to improve the ϵ_r and E_b of the nanocomposite.³²

Above all, the morphology design and surface treatment of inorganic fillers can greatly enhance the ϵ_r and U_e of nanocomposites.^{22,33} In addition, HfO_2 is a ferroelectric with high E_b , moderate ϵ_r (compared with SiO_2 and Al_2O_3) and wide band gap. Therefore, HfO_2 can act like a shell layer to reduce the field distortion and leakage current density, thereby improving the E_b of nanocomposites.³⁴ Inspired by that, we prepared 2D TiO_2 Ns by hydrothermal method. To decrease the difference in ϵ_r between TiO_2 Ns and polymer, HfO_2 acting as the passivation layer with high insulation and moderate ϵ_r coated on the TiO_2 Ns surface forms 2D core-shell nanosheets. HfO_2 @ TiO_2 nanosheets (HfO_2 @ TiO_2 Ns) make the nanocomposites with higher ϵ_r and lower dielectric loss than polymer matrix. Furthermore, HfO_2 @ TiO_2 Ns can establish an efficient barrier to inhibit the space charge conduction, and hamper the growing electric trees during the breakdown process.^{35,36} HfO_2 layer with high insulation could trap the charge carriers to hinder the mobility of charge carriers, and then improve the E_b . The 3 wt.% P(VDF-HFP)/ HfO_2 @ TiO_2 Ns sample presents a maximum U_e of 13.9 J/cm³ and charge-discharge efficiency of 55.1%.



Scheme 1. Schematic diagram of preparation of the 2D TiO_2 Ns and core-shell HfO_2 @ TiO_2 Ns.

2. Experimental

2.1. Preparation of TiO₂ Ns

TiO₂ Ns were prepared by a simple hydrothermal method^{37,38} as illustrated in Scheme 1. The TiO₂ Ns sample was obtained as follows: First, 25 mL tetrabutyl titanate (chemically pure) was added into a Teflon-lined with 2 mL of hydrofluoric acid (analytically pure, 40%) under magnetic stirring for 10 min to get a stable suspension. Subsequently, the suspension was reacted at 200 °C for 24 h and then cooled to room temperature. The resulting samples were washed with deionized water and ethanol, and then dried at 110 °C for 12 h.

2.2. Preparation of HfO₂@TiO₂ Ns

HfO₂@TiO₂ Ns were synthesized according to our previous work with slight modifications.³⁴ 0.3 g HfCl₄ (chemically pure) and 10 g TiO₂ Ns were added to a mixed solution (consisting of ethanol, CTAB powder and deionized water) and stirred for 2 h. The mixture was stirred at 80 °C, and the as-prepared gel was dried at 110 °C and calcined at 800 °C to remove the residual solvents and organics. The product was named as HfO₂@TiO₂ Ns.

2.3. Preparation of P(VDF-HFP)/HfO₂@TiO₂ nanocomposites

The P(VDF-HFP)/HfO₂@TiO₂ nanocomposites were prepared in the following process. First, 0.3 g poly(vinylidene fluoride-co-hexafluoropropylene) (P(VDF-HFP)) was dissolved in 10 mL DMF before the required amount of TiO₂ Ns

was added. The suspension was ultrasonicated for 30 min and vigorously stirred. Second, the P(VDF-HFP) and HfO₂@TiO₂ Ns suspension was cast onto the glass slides and dried at 70 °C for several hours to remove the solvent completely. Finally, all the composites were treated at 180 °C to eliminate the potential defects. For comparison purposes, P(VDF-HFP)/TiO₂ Ns nanocomposites without HfO₂ shell were prepared in the same procedure.

2.4. Characterization

X-ray diffraction (XRD) patterns were performed on a Bruker D8 ADVANCE diffractometer in the range of 10°–80° with Cu K α radiation. The transmission electron microscopy (TEM) was performed using a JEM-F200. Scanning electron microscopy (SEM) was measured by a Quanta FEG 250. The dielectric performance was performed using a Novocontrol Concept 80 impedance analyzer with an applied voltage of 1 V and ranging from 1 Hz to 1 MHz. E_b obtained by the RK2674B at a rate of 200 V/s. D–E loops (100 Hz) are recorded via Premier II ferroelectric test system.

3. Results and Discussion

SEM images of three types of TiO₂ products with different reaction times are shown in Fig. 1. It can be seen that the TiO₂ presents a regular spherical morphology with 12 h reaction time. Along with the reaction time increasing, the morphology of TiO₂ gradually changes from spherical to regular 2D flake. Therefore, in this paper, TiO₂ Ns with hydrothermal

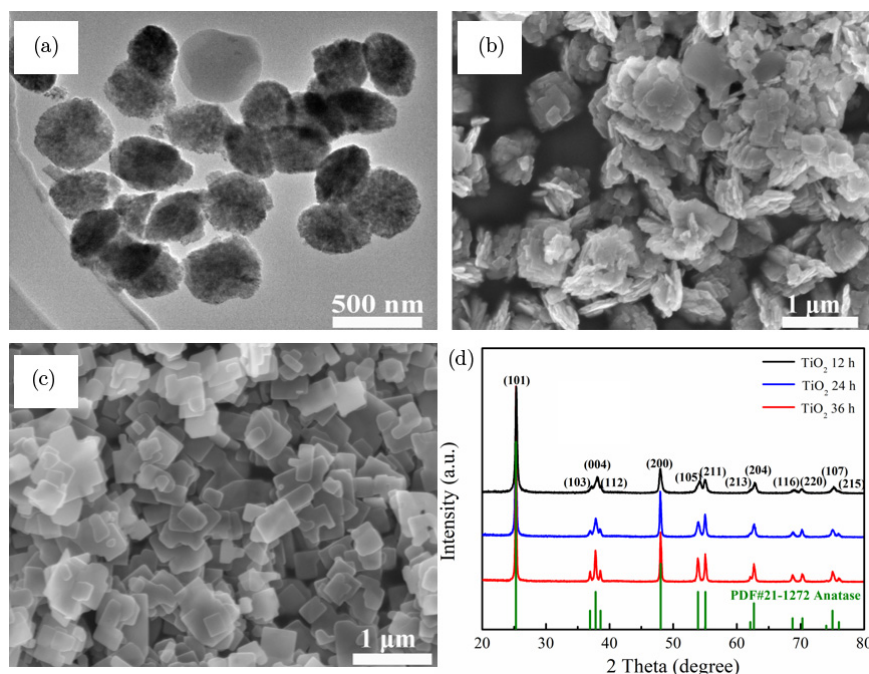


Fig. 1. SEM image of TiO₂ obtained with different reaction times: (a) 12 h, (b) 24 h and (c) 36 h. (d) XRD pattern of TiO₂.

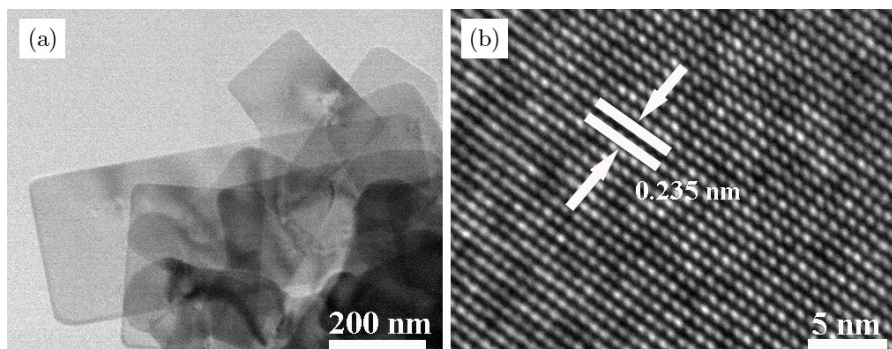


Fig. 2. (a) TEM image, (b) HR-TEM image of TiO₂ Ns.

reaction time of 36 h is selected as the inorganic filler of the nanocomposites. The obtained TiO₂ Ns shows a regular square shape with a side length of about 0.5–1 μm. And it is basically tiled on the surface of the conductive adhesive, indicating that its size is small in the thickness direction.

Figure 1(d) shows the XRD patterns of the TiO₂ Ns from the hydrothermal process in different reaction times. As the reaction time increases, the XRD diffraction peak becomes sharper. Moreover, TiO₂ Ns possesses a single-phase tetragonal structure without any impurities and all of the diffraction peaks can be perfectly corresponded to typical anatase structure (JCPDS No. 21-1272). To further study the structure of TiO₂ Ns, Figure 2 shows the TEM and HR-TEM images of TiO₂ Ns, the as-obtained TiO₂ Ns is semitransparent under the electron beam. It is indicated that the TiO₂ Ns was very thin and had large aspect ratios. The HR-TEM image shows that the lattice spacing of TiO₂ Ns is 0.235 nm.

The structure of HfO₂@TiO₂ Ns could be confirmed through the TEM, HR-TEM and XRD, as displayed in Fig. 3. Clearly, the HfO₂@TiO₂ Ns with a compact shell layer. In Fig. 3(c), TiO₂ Ns and HfO₂@TiO₂ Ns both exhibit a typical anatase structure and without any other impurities. The XRD peak intensity of HfO₂@TiO₂ Ns weakened after coating with HfO₂, which was attributed to the shielding effect of HfO₂. A similar phenomenon occurs in the literature with HfO₂@BT and SiO₂@SiC particles.^{34,39} Meanwhile, the homogeneity of HfO₂ and TiO₂ Ns could be further

confirmed by the elemental mapping analyses (Fig. 4), suggesting that a homogenous and tight HfO₂ layer is coated on the TiO₂ Ns surface.

The dispersion of the inorganic fillers is a major factor in dielectric properties for nanocomposites.⁴⁰ SEM images of 3 wt.% P(VDF-HFP)/HfO₂@TiO₂ are shown in Fig. 5, sheet-like HfO₂@TiO₂ Ns (indicated by the red dashed boxes) are mainly observed. The HfO₂@TiO₂ Ns can be well dispersed in the polymer without any obvious voids and interfacial flaws. It is indicated that these composites have high quality for the strong interfacial interaction between fillers and the matrix. Figure 5(b) shows the SEM micrographs of fractured surface of 3 wt.% P(VDF-HFP)/HfO₂@TiO₂ Ns. The results indicate that the HfO₂@TiO₂ Ns are parallelly oriented in the polymer matrix (indicated by the red arrows), which is good for improving the E_b of nanocomposites.

The ϵ_r may reflect the polarization characteristics in different conditions.⁴¹ The frequency dependence of ϵ_r and loss tangent for P(VDF-HFP)/HfO₂@TiO₂ Ns nanocomposites are summarized in Fig. 6(a). Clearly, the ϵ_r of P(VDF-HFP)/HfO₂@TiO₂ Ns was larger than that of polymer matrix because the HfO₂@TiO₂ Ns has a higher ϵ_r . In addition, stronger interfacial polarization with massive charges could accumulate at the fillers/matrix interface because of the difference in electrical performance between the fillers and matrix.⁴² For example, 15 wt.% P(VDF-HFP)/HfO₂@TiO₂ Ns illustrates the largest ϵ_r of 19.7 at 1 kHz (33.6 at 1 Hz).

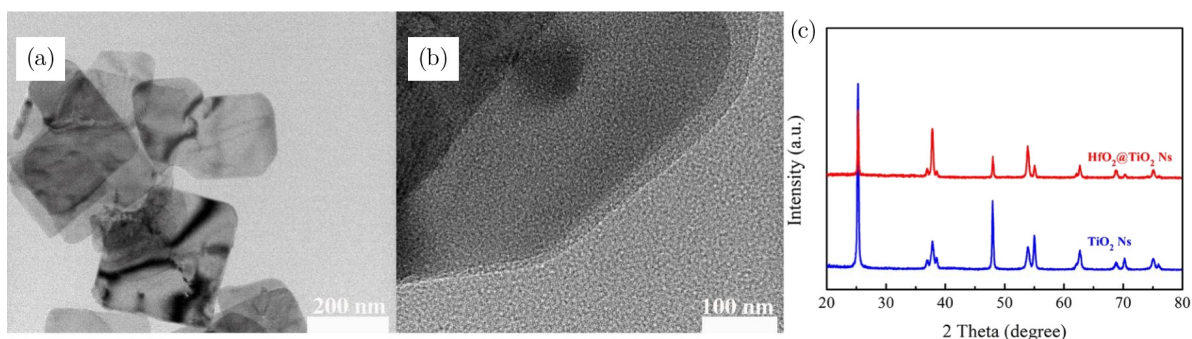


Fig. 3. (a) TEM image, (b) HR-TEM image of HfO₂@TiO₂ Ns. (c) XRD pattern of TiO₂ Ns and HfO₂@TiO₂ Ns.

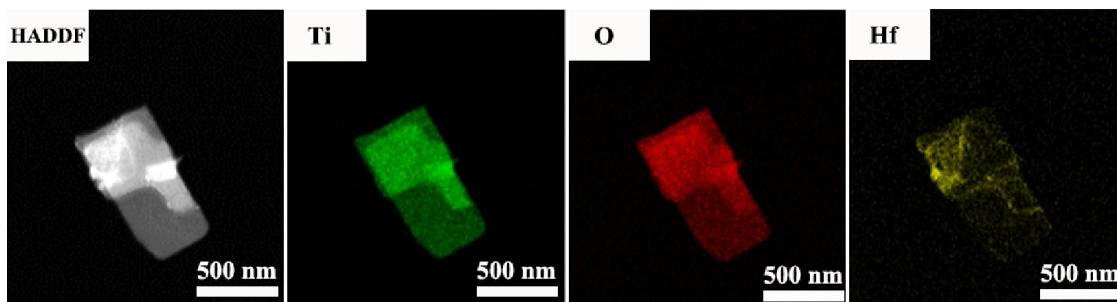


Fig. 4. EDS element mapping images of HfO₂@TiO₂ Ns.

Meanwhile, with the frequency increasing, the ϵ_r of nanocomposites presented a downtrend due to the delayed response of dipole.⁴³ In dielectrics, dielectric loss can be generally composed of the following parts: electrical polarization, interfacial polarization and dipole polarization. In Fig. 6(a), with the frequency increasing, loss tangent of all the nanocomposites decreases firstly and then increases. In nanocomposites, the loss tangent mainly comes from interfacial polarization and electronic conduction. The difference in electrical performance at interface region can cause strong interfacial polarization to increase the

dielectric loss.^{13,44} Meanwhile, in the semiconductor fillers of TiO₂ Ns with relatively high conductivity, the electronic conduction plays a major role in the nanocomposites.

To better evaluate the effect of the HfO₂ passivation layer for dielectric properties, a comparison of ϵ_r and loss tangent (@ 1 kHz) for nanocomposites is shown in Fig. 6(b). Obviously, the P(VDF-HFP)/HfO₂@TiO₂ Ns nanocomposites exhibit a relatively low ϵ_r and loss tangent, which may be due to the following factors. First, the shell of HfO₂ with moderate dielectric permittivity may relieve the dielectric mismatch of the interface region to decrease the interfacial

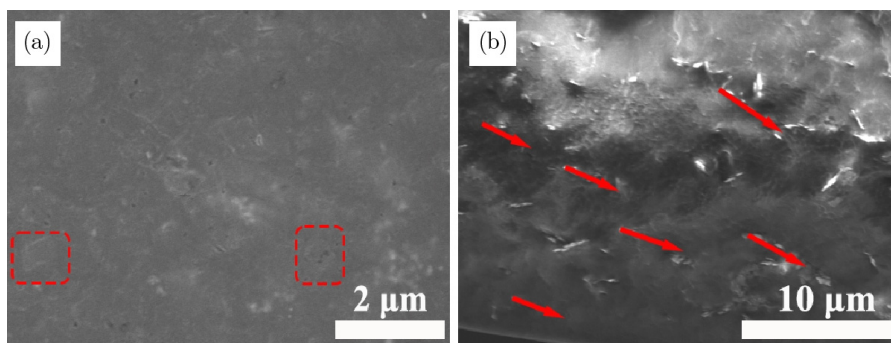


Fig. 5. (a) Top view and (b) cross-sectional SEM images of 3 wt.% P(VDF-HFP)/HfO₂@TiO₂ Ns nanocomposites.

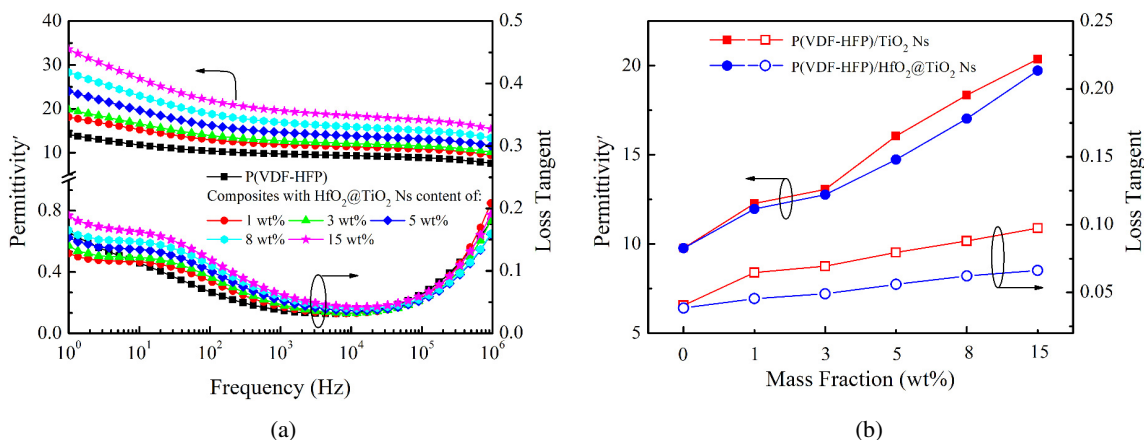


Fig. 6. (a) Frequency dependence of ϵ_r and loss tangent for nanocomposites. (b) Comparison of ϵ_r and loss tangent of nanocomposites of TiO₂ Ns and HfO₂@TiO₂ Ns at 1 KHz.

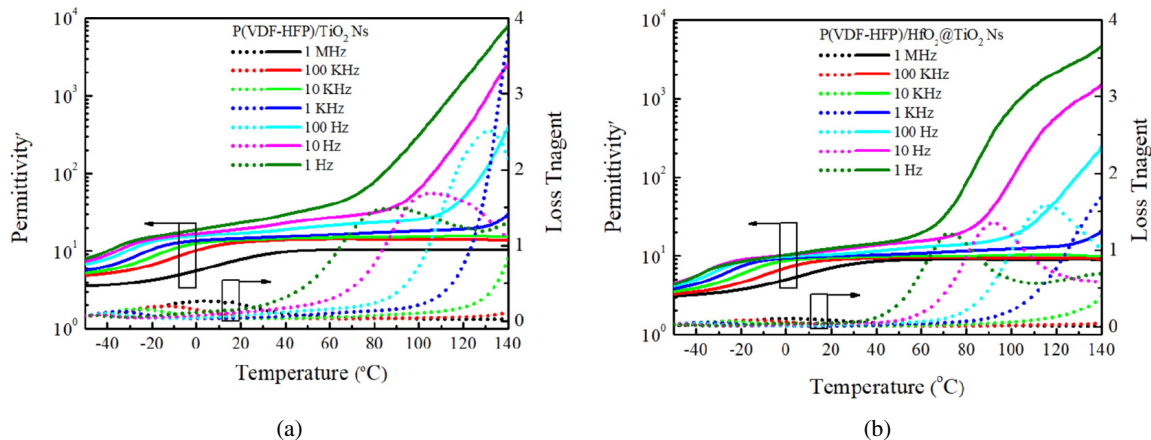


Fig. 7. Temperature dependence of the ϵ_r and loss tangent for the nanocomposites with 3 wt.% of (a) TiO_2 Ns and (b) $\text{HfO}_2@ \text{TiO}_2$ Ns.

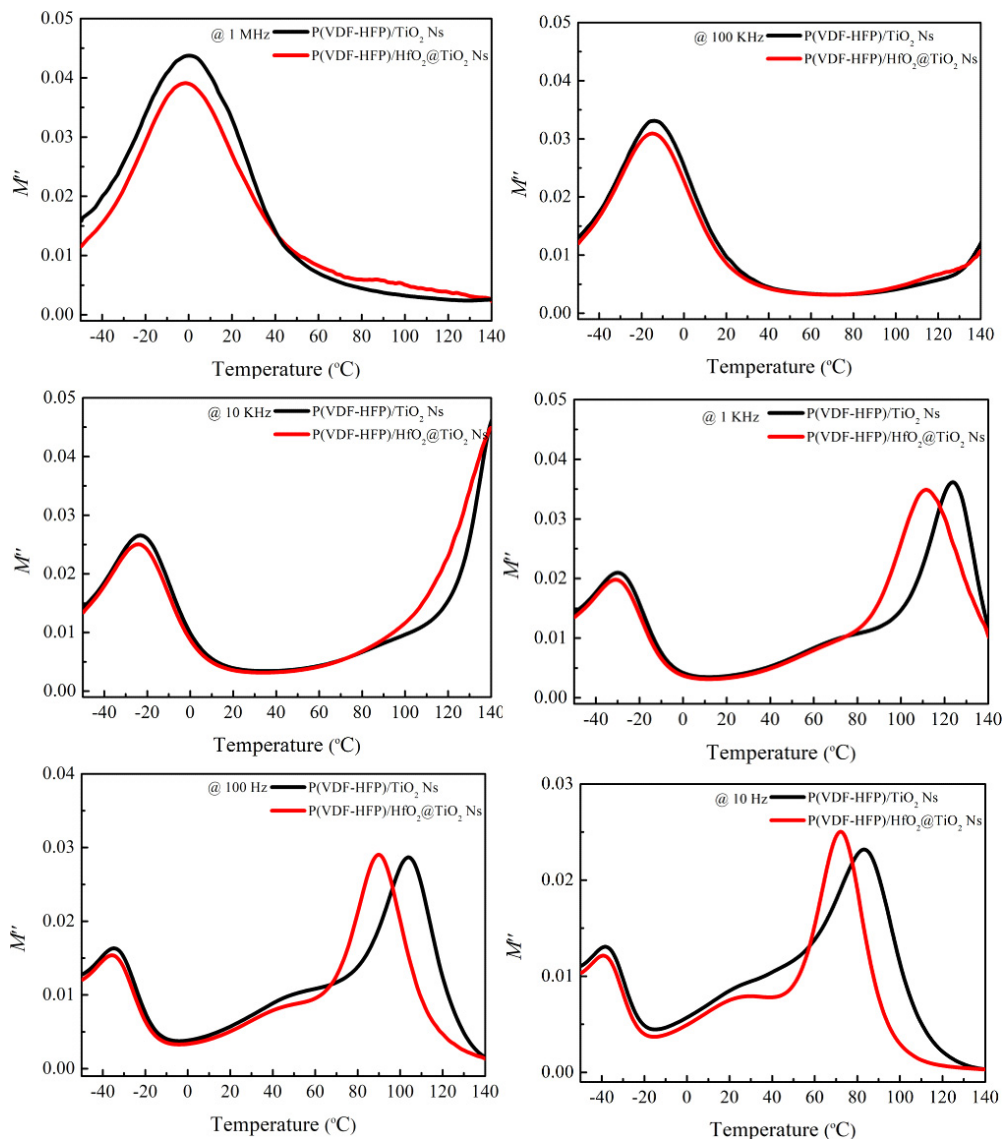


Fig. 8. Temperature dependence of M'' for the P(VDF-HFP) nanocomposites with 3 wt.% of TiO_2 Ns and $\text{HfO}_2@ \text{TiO}_2$ Ns.

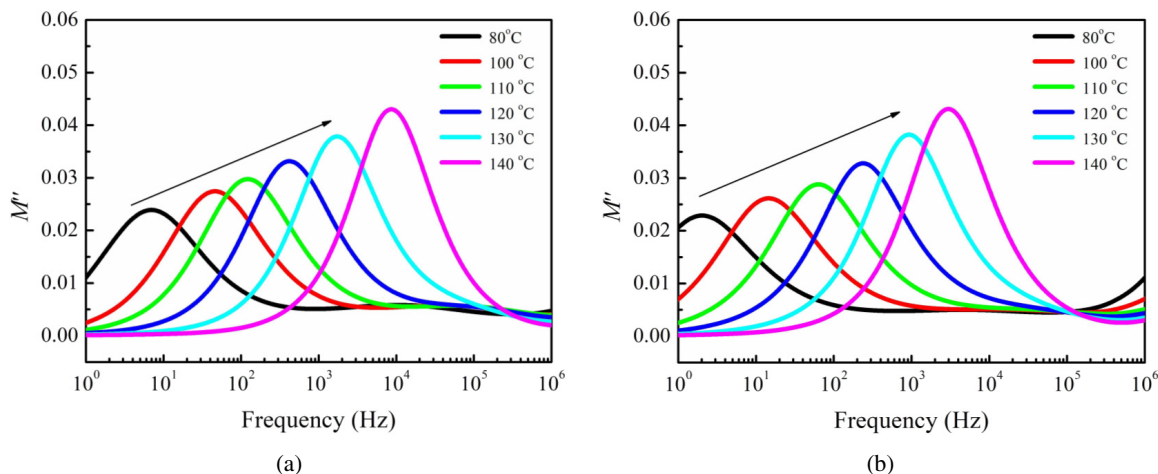


Fig. 9. Frequency dependence of M'' for P(VDF-HFP) nanocomposites with 3 wt.%: (a) TiO_2 Ns and (b) $\text{HfO}_2@/\text{TiO}_2$ Ns.

polarization. Second, the amorphous HfO_2 shell with highly insulating acting as a passivation layer can effectively suppress the charge migration to reduce the space charge polarization.

As shown in Fig. 7, to further evaluate the dielectric behavior of these nanocomposites, we provide the temperature dependence of the ϵ_r and loss tangent for the nanocomposites. It can be found that at low frequency (1 Hz), the ϵ_r for two nanocomposites shows obvious relaxation peak at about -20°C , which is caused by the T_g of polymer. With the frequency increasing, the relaxation peak gradually moves toward high temperature, owing to the internal segments of the polymer requiring more energy to complete the motion at high frequency.⁴⁵ In addition, the difference between the two nanocomposites becomes more obvious with the increase of temperature, the loss tangent of P(VDF-HFP)/ $\text{HfO}_2@/\text{TiO}_2$ Ns is obviously smaller than P(VDF-HFP)/ TiO_2 Ns. It is mainly because the high insulation buffer layer HfO_2 can significantly reduce the conduction loss. It indicated the

core-shell $\text{HfO}_2@/\text{TiO}_2$ Ns can improve the ϵ_r and restrain the dielectric loss of nanocomposites.

The dielectric loss of nanocomposites increased dramatically at elevated temperature, which will cover other loss mechanisms. Interpreting the dielectric relaxation data by electrical modulus is an effective method. The real and imaginary parts of modulus (M' and M'') can be calculated as follows:

$$M' = \frac{\epsilon'}{\epsilon'^2 + \epsilon''^2}; \quad M'' = \frac{M''}{M'^2 + M''^2}. \quad (3)$$

Figure 8 shows the temperature dependence of M'' for nanocomposites with 3% fillers at various frequencies. We can see only one relaxation peak in the high-frequency region. It is due to the molecular motions in the crystalline region of P(VDF-HFP). In polymer nanocomposites, the interfacial polarization is attributed to the differences in conductivity of inorganic fillers, crystalline and amorphous regions. With the reduction of frequency, in addition to the α relaxation, another relaxation peak appears at high temperature attributed to the interfacial polarization.^{46–48}

The M'' of nanocomposites filled with 3 wt.% of TiO_2 Ns and $\text{HfO}_2@/\text{TiO}_2$ Ns is shown in Figs. 9(a) and 9(b). As the temperature increases, the M'' peaks for the interfacial polarization process move to a higher frequency. This phenomenon is correlated with the charges blocked on the inorganic fillers (or crystalline regions)/amorphous boundaries.

Interfacial polarization can be represented by the Arrhenius behavior and the activation energy (E_a) of charge carriers hopping could be calculated from the following equation:

$$\ln f_{\max} = \ln f_0 - \frac{E_a}{kT}, \quad (4)$$

where f_0 is the pre-exponential factor, k is the Boltzmann constant, T is the temperature. Figure 10 shows the Arrhenius plots of the variation of $\ln(f_{\max})$ with the inverse of temperature ($1000/T$) for the nanocomposites with 3 wt.% fillers.

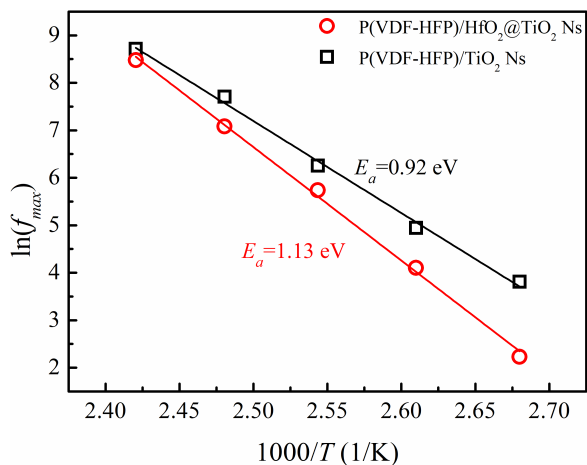


Fig. 10. Activation energy plots of P(VDF-HFP)/ TiO_2 Ns and P(VDF-HFP)/ $\text{HfO}_2@/\text{TiO}_2$ Ns samples.

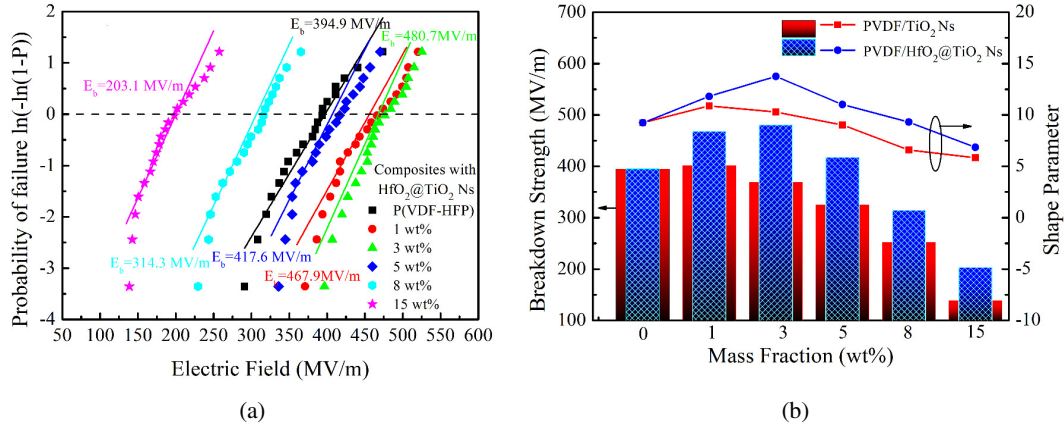


Fig. 11. Weibull distribution of E_b for P(VDF-HFP) nanocomposites; (b) The E_b of the nanocomposites with different contents of TiO₂ Ns and HfO₂@TiO₂ Ns.

The calculated E_a of P(VDF-HFP)/HfO₂@TiO₂ Ns is higher than P(VDF-HFP)/TiO₂ Ns. It indicates that the passivation shell layer of HfO₂ could effectively limit the free electrons migrations and enhance the E_b and U_e .⁴³

In order to analyze the breakdown failure behavior of these nanocomposites, the E_b and electric failure $P(E)$ are described as follows:

$$P(E) = 1 - \exp\left(-\left(\frac{E}{E_b}\right)^\beta\right), \quad (5)$$

where E and β are the experimental E_b and shape parameter, respectively. Figure 11(a) shows the Weibull distribution plots of E_b for nanocomposites with different contents of

HfO₂@TiO₂ Ns. The E_b increases from 394.9 MV/m to 480.7 MV/m as the HfO₂@TiO₂ Ns increases to 3 wt.%. Further, the E_b of 15 wt.% nanocomposites dramatically decreases to 203.1 MV/m. The E_b of nanocomposites with various filler contents is summarized in Fig. 11(b). All of the nanocomposites exhibit a higher β value, confirming the nanocomposites with high quality and stability.⁴⁹ In addition, the β value and E_b of the P(VDF-HFP)/HfO₂@TiO₂ Ns are larger than that of the P(VDF-HFP)/TiO₂ Ns. The E_b of the 3 wt.% P(VDF-HFP)/HfO₂@TiO₂ Ns (480.7 MV/m) is about 1.3 times that of the 3 wt.% P(VDF-HFP)/TiO₂ Ns (368.6 MV/m). The improvement of the E_b for nanocomposites by HfO₂ shell is attributed to the following

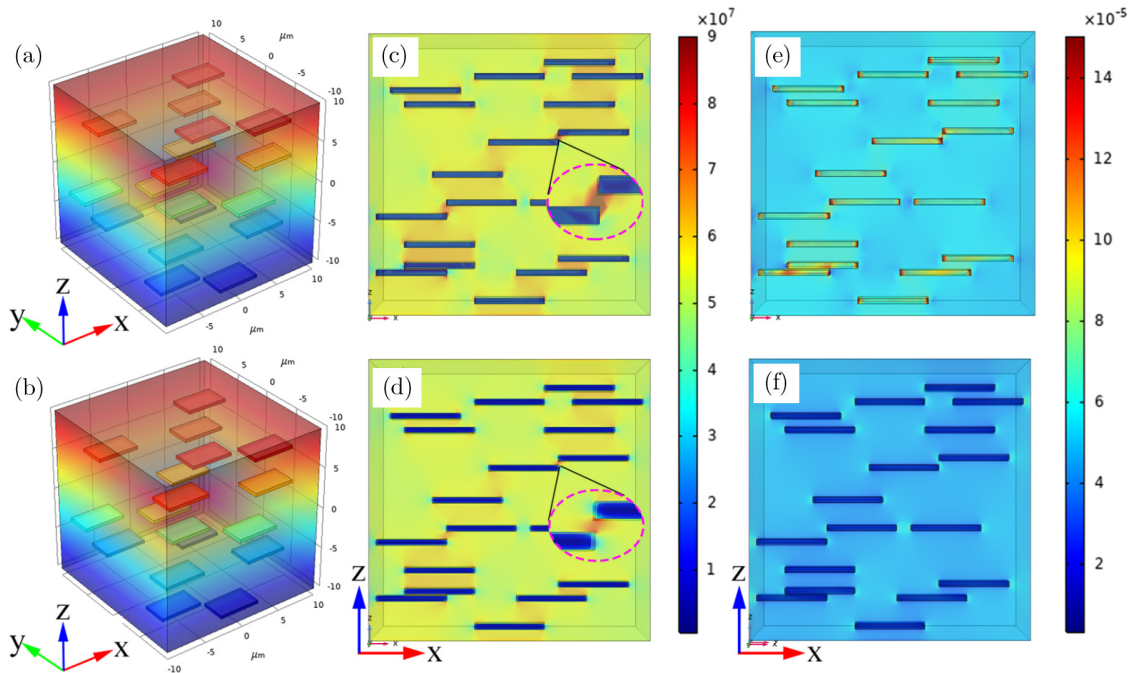


Fig. 12. The (a), (b) voltage, (c), (d) electric field redistribution, (e), (f) current density of 3 wt.% P(VDF-HFP)/TiO₂ and P(VDF-HFP)/HfO₂@TiO₂ nanocomposite.

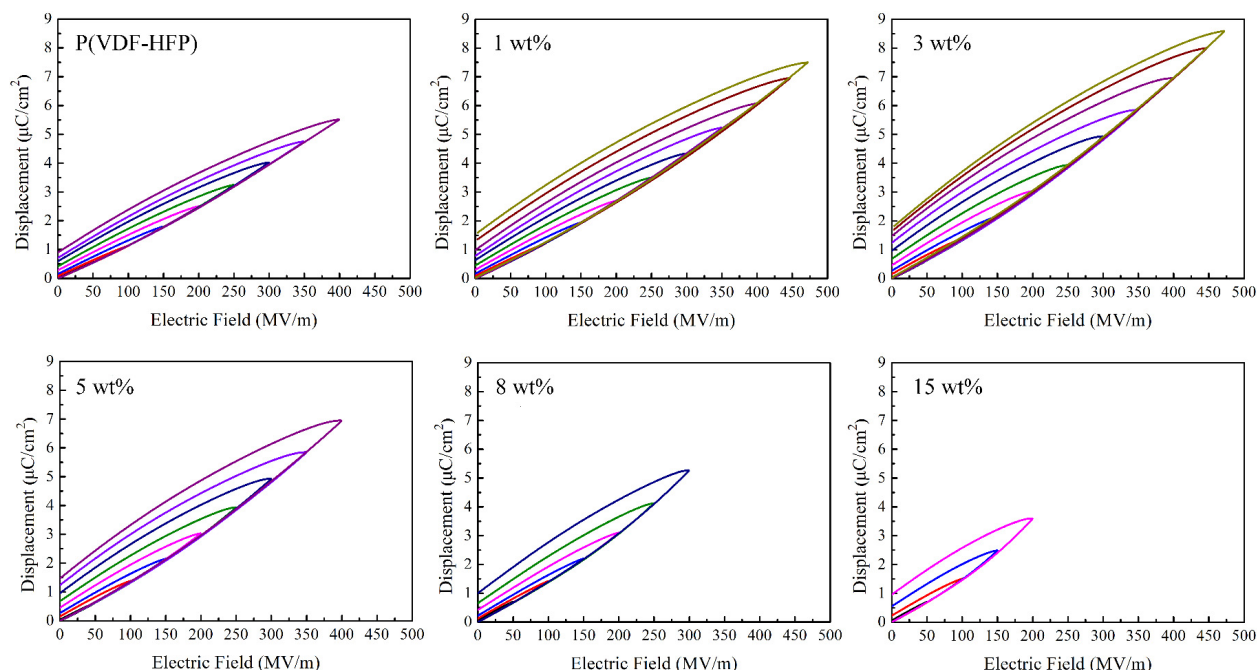


Fig. 13. D–E loops of P(VDF-HFP)-based nanocomposites.

factors. First, the $\text{HfO}_2@TiO_2$ Ns can establish an efficient barrier to limit the space charge conduction, and hamper the growing electric trees during the breakdown process. Second, the HfO_2 acting as a passivation layer with moderate ϵ_r can also effectively alleviate the electric mismatch between the matrix and fillers. Third, the HfO_2 layer with high insulation could hinder the mobility of charge carriers, and then improve the E_b .^{15,50}

In order to further study the electrical breakdown mechanism of P(VDF-HFP) nanocomposites filled with TiO_2 Ns and $\text{HfO}_2@TiO_2$ Ns, the electric field distribution and leakage current density of nanocomposites were analyzed through finite element simulation by COMSOL Multiphysics, as depicted in Fig. 12. The fillers were uniformly dispersed in matrix, and the ϵ_r of P(VDF-HFP), TiO_2 Ns and HfO_2 were set as around 10, 50 and 25, respectively. First, the electric potential of nanocomposite is deduced (Figs. 12(a) and 12(b)). Figures 12(c) and 12(d) give the distribution of electric field strength, the local electric field strength in nanocomposite with $\text{HfO}_2@TiO_2$ Ns is much lower than that of nanocomposite with TiO_2 Ns. From the high-magnification image of electric field strength, we can clearly see that the field distortion mainly located in tips of the two adjacent TiO_2 Ns, and the local electric field of TiO_2 Ns is significantly higher than that of $\text{HfO}_2@TiO_2$ Ns. This is due to the fact that HfO_2 shell can facilitate alleviation of the field strength because of the HfO_2 with moderate dielectric permittivity (~ 25). In other words, the HfO_2 shell acts as a passivation layer to redistribution of the electric field between the high ϵ_r fillers and the low ϵ_r polymer matrix and thus avoids

breakdown under high electric field. Moreover, suppressing leakage current can help improve the E_b .^{3,50} The current density of nanocomposites filled with 3 wt.% TiO_2 Ns and $\text{HfO}_2@TiO_2$ Ns is displayed in Figs. 12(e) and 12(f). The P(VDF-HFP)/ $\text{HfO}_2@TiO_2$ Ns nanocomposites showed a relatively lower local current density, the HfO_2 coated on the TiO_2 surface to restrict the overall current. Therefore, the results further verified the conclusion that the passivation layer of HfO_2 shell could enhance the E_b for nanocomposites.

The D–E loops of the P(VDF-HFP)/ $\text{HfO}_2@TiO_2$ Ns are given in Fig. 13. With the increase of $\text{HfO}_2@TiO_2$ Ns content, the D_{max} of the nanocomposites increases and the E_b increases

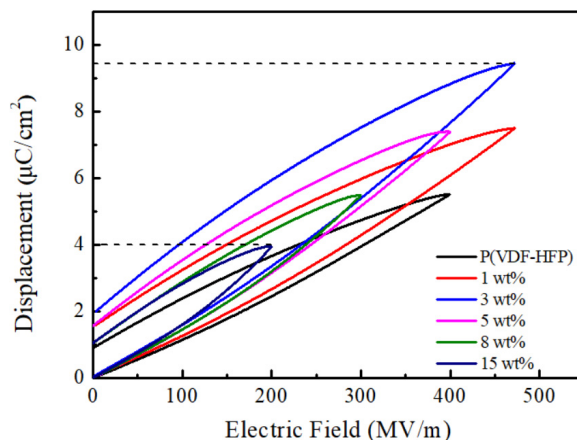


Fig. 14. D–E loops of P(VDF-HFP)/ $\text{HfO}_2@TiO_2$ Ns nanocomposites at maximum electric field.

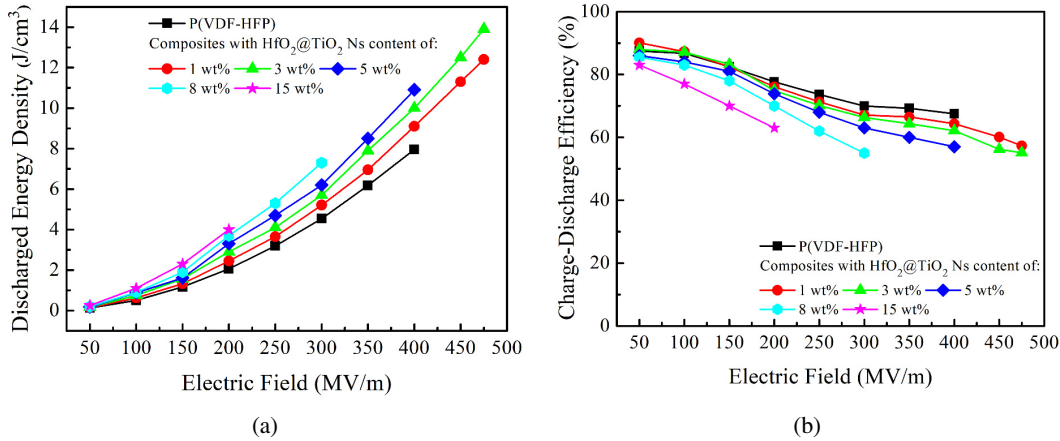


Fig. 15. The (a) U_e and (b) η of P(VDF-HFP)/HfO₂@TiO₂ Ns nanocomposite.

first and then decreases (as indicated by Fig. 14). After introducing HfO₂@TiO₂ Ns, the D_{max} of nanocomposites increases remarkably. The significantly enhanced D_{max} of P(VDF-HFP)/HfO₂@TiO₂ Ns nanocomposites owing to the increased E_b and ϵ_r . For example, 3 wt.% P(VDF-HFP)/HfO₂@TiO₂ Ns has the largest D_{max} of 9.4 $\mu\text{C}/\text{cm}^2$, which is 1.7 times of pristine P(VDF-HFP) (5.5 $\mu\text{C}/\text{cm}^2$).

The U_e and charge–discharge efficiency (η) of the nanocomposites are calculated and shown in Fig. 15(a). According to Eq. (2), the E_b has a greater influence on the U_e . Therefore, 3 wt.% P(VDF-HFP)/HfO₂@TiO₂ Ns represents the largest U_e of 13.9 J/cm³, which is 1.7 times that of matrix. The η can be expressed as $\eta = U_e/U \times 100\%$, it is also a critical parameter in energy storage equipment. It can be found that the introduction of HfO₂@TiO₂ Ns will cause a slight increase in the remanent displacement, which causes a decrease in η . As shown in Fig. 15(b), η of nanocomposite is slightly lower than polymer matrix. The η of 3 wt.% P(VDF-HFP)/HfO₂@TiO₂ Ns nanocomposite is 55.1% at 475 MV/m.

To demonstrate the advantage of the 2D HfO₂@TiO₂ Ns, the U_e and η of nanocomposites as an instance for

comparison are shown in Fig. 16. The U_e of P(VDF-HFP)/HfO₂@TiO₂ Ns is 13.9 J/cm³ almost 1.6 times of corresponding P(VDF-HFP)/TiO₂ Ns nanocomposite (8.9 J/cm³). Meanwhile, 3 wt.% P(VDF-HFP)/HfO₂@TiO₂ Ns shows a high η of 62.1% while the corresponding P(VDF-HFP)/TiO₂ Ns is only 52.3% at 400 MV/m. Even at the maximum electric field of 475 MV/m, the η of P(VDF-HFP)/HfO₂@TiO₂ nanocomposite remains at 55.1%.

4. Conclusions

In conclusion, HfO₂@TiO₂ Ns have been successfully designed and constructed by combining the high ϵ_r 2D TiO₂ Ns and HfO₂ passivation layer. The high aspect ratio of HfO₂@TiO₂ Ns in the polymer matrix can not only enhance ϵ_r , but also establish a potential barrier to limit the migration of charges. The HfO₂ layer leads to a uniform distribution of electric field and the high insulation HfO₂ layer can also inhibit dielectric loss and current density. The finite element results further show that the passivation layer of HfO₂ can

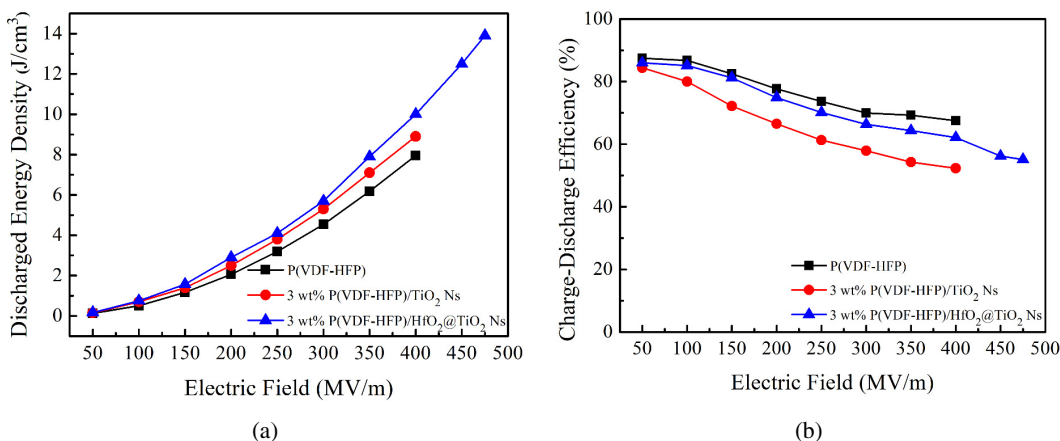






Fig. 16. Comparison of (a) U_e and (b) η for pristine P(VDF-HFP) and 3 wt.% P(VDF-HFP)-based nanocomposites.

redistribute the electric field and suppress the current density to improve the E_b and U_e . A high U_e of 13.9 J/cm^3 was accessed for 3 wt.% P(VDF-HFP)/ HfO_2 @ TiO_2 Ns sample at 475 MV/m. This research provides an efficient strategy for the development of high U_e polymer-based dielectrics, with the expectation of applying them to advanced power electronics systems.

Acknowledgments

This work was supported by the Key Research and Development Plan of Shaanxi Province (2021GY-251, 2021GY-219).

ORCID

Chao Chen  <https://orcid.org/0000-0002-6496-0962>
 Chen Guo  <https://orcid.org/0009-0000-0760-4497>
 Xiaoyong Wei  <https://orcid.org/0000-0001-9677-4227>
 Pengfei Wang  <https://orcid.org/0000-0002-5285-9832>

References

- S. Koohi-Fayegh and M. A. Rosen, A review of energy storage types, applications and recent developments, *J. Energy Storage* **27**, 101047 (2020).
- L. T. Yang, X. Kong, F. Li, H. Hao, Z. X. Cheng, H. X. Liu, J. F. Li and S. J. Zhang, Perovskite lead-free dielectrics for energy storage applications, *Prog. Mater. Sci.* **102**, 72 (2019).
- M. J. Feng, Y. Feng, T. D. Zhang, J. L. Li, Q. G. Chen, Q. G. Chi and Q. Q. Lei, Recent advances in multilayer-structure dielectrics for energy storage application, *Adv. Sci.* **8**, 2102221 (2021).
- H. B. Zhang, M. A. Marwat, B. Xie, M. Ashtar, K. Liu, Y. W. Zhu, L. Zhang, P. Y. Fan, C. Samart and Z. G. Ye, Polymer matrix nanocomposites with 1D ceramic nanofillers for energy storage capacitor applications, *ACS Appl. Mater. Inter.* **12**, 1 (2020).
- L. Dou, Y. H. Lin and C. W. Nan, An overview of linear dielectric polymers and their nanocomposites for energy storage, *Molecules* **26**, 6148 (2021).
- Y. L. Qiao, X. D. Yin, T. Y. Zhu, H. Li and C. B. Tang, Dielectric polymers with novel chemistry, compositions and architectures, *Prog. Polym. Sci.* **80**, 153 (2018).
- J. S. Ho and S. G. Greenbaum, Polymer capacitor dielectrics for high temperature applications, *ACS Appl. Mater. Inter.* **10**, 29189 (2018).
- X. Zhang, B. W. Li, L. J. Dong, H. X. Liu, W. Chen, Y. Shen and C. W. Nan, Superior energy storage performances of polymer nanocomposites via modification of filler/polymer interfaces, *Adv. Mater. Interfaces* **5**, 1800096 (2018).
- F. E. Bouharras, M. Raihane and B. Ameduri, Recent progress on core-shell structured BaTiO_3 @polymer/fluorinated polymers nanocomposites for high energy storage: Synthesis, dielectric properties and applications, *Prog. Mater. Sci.* **113**, 100670 (2020).
- Z. B. Pan, L. M. Yao, G. L. Ge, B. Shen and J. W. Zhai, High-performance capacitors based on NaNbO_3 nanowires/poly(vinylidene fluoride) nanocomposites, *J. Mater. Chem. A* **6**, 14614 (2018).
- S. Adireddy, V. S. Puli, S. C. Sklare, T. J. Lou, B. C. Riggs, R. Elupula, S. M. Grayson and D. B. Chrisey, PVDF- BaSrTiO_3 nanocomposites for flexible electrical energy storage devices, *Emerg. Mater. Res.* **3**, 265 (2014).
- Q. G. Chi, X. B. Wang, C. H. Zhang, Q. G. Chen, M. H. Chen, T. D. Zhang, L. Gao, Y. Zhang, Y. Cui, X. Wang and Q. Q. Lei, High energy storage density for Poly(vinylidene fluoride) composites by introduced core-shell $\text{CaCu}_3\text{Ti}_4\text{O}_{12}$ @ Al_2O_3 nanofibers, *ACS Sustain. Chem. Eng.* **6**, 8641 (2018).
- Z. M. Dang, J. K. Yuan, J. W. Zha, T. Zhou, S. T. Li and G. H. Hu, Fundamentals, processes and applications of high-permittivity polymer matrix composites, *Prog. Mater. Sci.* **57**, 660 (2012).
- H. Luo, X. F. Zhou, C. Ellingford, Y. Zhang, S. Chen, K. C. Zhou, D. Zhang, C. R. Bowen and C. Y. Wan, Interface design for high energy density polymer nanocomposites, *Chem. Soc. Rev.* **48**, 4424 (2019).
- M. H. Yang, Q. M. Li, X. M. Zhang, E. Bilotti, C. Zhang, C. Xu, S. H. Gan and Z. M. Dang, Surface engineering of 2D dielectric polymer films for scalable production of high-energy-density films, *Prog. Mater. Sci.* **128**, 100968 (2022).
- Y. Zhou, C. Yuan, S. J. Wang, Y. J. Zhu, S. Cheng, X. Yang, Y. Yang, J. Hu, J. L. He and Q. Li, Interface-modulated nanocomposites based on polypropylene for high-temperature energy storage, *Energy Storage Mater.* **28**, 255 (2020).
- S. Kango, S. Kalia, A. Celli, J. Njuguna, Y. Habibi and R. Kumar, Surface modification of inorganic nanoparticles for development of organic-inorganic nanocomposites — A review, *Prog. Polym. Sci.* **38**, 1232 (2013).
- L. Y. Xie, X. Y. Huang, Y. H. Huang, K. Yang and P. K. Jiang, Core@double-shell structured BaTiO_3 -polymer nanocomposites with high dielectric constant and low dielectric loss for energy storage application, *J. Phys. Chem. C* **117**, 22525 (2013).
- S. H. Liu, S. X. Xue, B. Shen and J. W. Zhai, Reduced energy loss in poly(vinylidene fluoride) nanocomposites by filling with a small loading of core-shell structured $\text{BaTiO}_3/\text{SiO}_2$ nanofibers, *Appl. Phys. Lett.* **107**, 032907 (2015).
- L. Y. Xie, X. Y. Huang, C. Wu and P. K. Jiang, Core-shell structured poly(methyl methacrylate)/ BaTiO_3 nanocomposites prepared by *in situ* atom transfer radical polymerization: A route to high dielectric constant materials with the inherent low loss of the base polymer, *J. Mater. Chem.* **21**, 5897 (2011).
- S. H. Liu, J. Wang, H. S. Hao, L. M. Zhao and J. W. Zhai, Discharged energy density and efficiency of nanocomposites based on poly(vinylidene fluoride) and core-shell structured BaTiO_3 @ Al_2O_3 nanoparticles, *Ceram. Int.* **44**, 22850 (2018).
- H. Li, F. H. Liu, B. Y. Fan, D. Ai, Z. R. Peng and Q. Wang, Nanostructured ferroelectric-polymer composites for capacitive energy storage, *Small Methods* **2**, 1700399 (2018).
- D. L. He, Y. Wang, L. Y. Zhang, S. L. Song and Y. Deng, Poly(vinylidene fluoride)-Based composites modulated via multiscale two-dimensional fillers for high dielectric performances, *Compos. Sci. Technol.* **159**, 162 (2018).
- K. Prabakaran, S. Mohanty and S. K. Nayak, Influence of surface modified TiO_2 nanoparticles on dielectric properties of PVDF-HFP nanocomposites, *J. Mater. Sci.: Mater. Electron.* **25**, 4590 (2014).
- J. J. Xu, C. Fu, H. Y. Chu, J. Qian, W. Y. Li, X. H. Ran and W. Nie, Improved discharge energy density of poly(vinylidene fluoride)-based nanocomposites via a small amount of dopamine-modified TiO_2 nanosheets, *J. Electron. Mater.* **50**, 4250 (2021).

- ²⁶U. Diebold, The surface science of titanium dioxide, *Surf. Sci. Rep.* **48**, 53 (2003).
- ²⁷S. W. Liu, J. G. Yu and M. Jaroniec, Tunable photocatalytic selectivity of hollow TiO₂ microspheres composed of anatase polyhedra with exposed [001] facets, *J. Am. Chem. Soc.* **132**, 11914 (2010).
- ²⁸X. G. Han, Q. Kuang, M. S. Jin, Z. X. Xie and L. S. Zheng, Synthesis of titania nanosheets with a high percentage of exposed [001] facets and related photocatalytic properties, *J. Am. Chem. Soc.* **131**, 3152 (2009).
- ²⁹D. V. Bavykin, J. M. Friedrich and F. C. Walsh, Protonated titanates and TiO₂ nanostructured materials: Synthesis, properties, and applications, *Adv. Mater.* **18**, 2807 (2006).
- ³⁰M. Jang, S. Y. Park, S. K. Kim, D. Jung, W. Song, S. Myung, S. S. Lee, D. H. Yoon and K. S. An, Strategic customization of polymeric nanocomposites modified by 2D titanium oxide nanosheet for high-*k* and flexible gate dielectrics, *Small* **17**, 2007213 (2021).
- ³¹G. Jian, Y. Jiao, L. Feng, Q. Z. Meng, N. Yang, S. T. Zhu, M. F. Lu and C. P. Wong, High energy density of BaTiO₃@TiO₂ nanosheet/polymer composites via ping-pong-like electron area scattering and interface engineering, *NPG Asia Mater.* **14**, 4 (2022).
- ³²Y. K. Zhu, H. Yao, P. K. Jiang, J. D. Wu, X. Zhu and X. Y. Huang, Two-dimensional high-*k* nanosheets for dielectric polymer nanocomposites with ultrahigh discharged energy density, *J. Phys. Chem. C* **122**, 18282 (2018).
- ³³M. F. Guo, J. Y. Jiang, Z. H. Shen, Y. H. Lin, C. W. Nan and Y. Shen, High-energy-density ferroelectric polymer nanocomposites for capacitive energy storage: Enhanced breakdown strength and improved discharge efficiency, *Mater. Today* **29**, 49 (2019).
- ³⁴C. Chen, Y. C. Xie, J. J. Liu, J. Li, X. Y. Wei and Z. C. Zhang, Enhanced energy storage capability of P(VDF-HFP) nanodielectrics by HfO₂ passivation layer: Preparation, performance and simulation, *Compos. Sci. Technol.* **188**, 107968 (2020).
- ³⁵S. B. Luo, J. Y. Yu, S. H. Yu, R. Sun, L. Q. Cao, W. H. Liao and C. P. Wong, Significantly enhanced electrostatic energy storage performance of flexible polymer composites by introducing highly insulating-ferroelectric microhybrids as fillers, *Adv. Energy Mater.* **9**, 1803204 (2019).
- ³⁶H. Li, D. Ai, L. L. Ren, B. Yao, Z. B. Han, Z. H. Shen, J. J. Wang, L. Q. Chen and Q. Wang, Scalable polymer nanocomposites with record high-temperature capacitive performance enabled by rationally designed nanostructured inorganic fillers, *Adv. Mater.* **31** (2019).
- ³⁷K. M. Chen, Z. Jiang, J. L. Qin, Y. Jiang, R. Li, H. Tang and X. F. Yang, Synthesis and improved photocatalytic activity of ultrathin TiO₂ nanosheets with nearly 100% exposed [001] facets, *Ceram. Int.* **40**, 16817 (2014).
- ³⁸X. J. Lu, X. L. Mou, J. J. Wu, D. W. Zhang, L. L. Zhang, F. Q. Huang, F. F. Xu and S. M. Huang, Improved-performance dye-sensitized solar cells using Nb-doped TiO₂ electrodes: Efficient electron injection and transfer, *Adv. Funct. Mater.* **20**, 509–515 (2010).
- ³⁹J. Y. Bi, Y. Z. Gu, Z. C. Zhang, S. K. Wang, M. Li and Z. G. Zhang, Core-shell SiC/SiO₂ whisker reinforced polymer composite with high dielectric permittivity and low dielectric loss, *Mater. Design* **89**, 933 (2016).
- ⁴⁰B. Lin, Z. T. Li, Y. Yang, Y. Li, J. C. Lin, X. M. Zheng, F. A. He and K. H. Lam, Enhanced dielectric permittivity in surface-modified graphene/PVDF composites prepared by an electrospinning-hot pressing method, *Compos. Sci. Technol.* **172**, 58 (2019).
- ⁴¹X. Lu, X. W. Zou, J. L. Shen, L. Zhang, L. Jin and Z. Y. Cheng, High energy density with ultrahigh discharging efficiency obtained in ceramic-polymer nanocomposites using a non-ferroelectric polar polymer as matrix, *Nano Energy* **70**, 104551 (2020).
- ⁴²Q. Huang, H. Luo, C. Chen, X. F. Zhou, K. C. Zhou and D. Zhang, Enhanced energy density in P(VDF-HFP) nanocomposites with gradient dielectric fillers and interfacial polarization, *J. Alloy Compd.* **696**, 1220 (2017).
- ⁴³C. V. Channal and J. P. Jog, Dielectric relaxations in PVDF/BaTiO₃ nanocomposites, *Express Polym. Lett.* **2**, 294 (2008).
- ⁴⁴X. Y. Huang and P. K. Jiang, Core-shell structured high-*k* polymer nanocomposites for energy storage and dielectric applications, *Adv. Mater.* **27**, 546 (2015).
- ⁴⁵Z. H. Dai, T. Li, Y. Gao, J. Xu, J. L. He, Y. X. Weng and B. H. Guo, Achieving high dielectric permittivity, high breakdown strength and high efficiency by cross-linking of poly(vinylidene fluoride)/BaTiO₃ nanocomposites, *Compos. Sci. Technol.* **169**, 142 (2019).
- ⁴⁶M. W. Yao, S. Y. You and Y. Peng, Dielectric constant and energy density of poly(vinylidene fluoride) nanocomposites filled with core-shell structured BaTiO₃@Al₂O₃ nanoparticles, *Ceram. Int.* **43**, 3127 (2017).
- ⁴⁷H. Rekik, Z. Ghallabi, I. Royaud, M. Arous, G. Seytre, G. Boiteux and A. Kallel, Dielectric relaxation behaviour in semi-crystalline polyvinylidene fluoride (PVDF)/TiO₂ nanocomposites, *Compos. Part B: Eng.* **45**, 1199 (2013).
- ⁴⁸N. X. Xu, L. Hu, Q. L. Zhang, X. R. Xiao, H. Yang and E. J. Yu, Significantly enhanced dielectric performance of poly(vinylidene fluoride-co-hexafluoropylene)-based composites filled with hierarchical flower-like TiO₂ particles, *ACS Appl. Mater. Inter.* **7**, 27373 (2015).
- ⁴⁹H. Kojima, Y. Otake, T. Takahashi, N. Hayakawa, K. Hasegawa, H. Saito and M. Sakaki, Analysis of conditioning and damaging process in vacuum based on breakdown probability distribution, *IEEE. Trans. Dielectr. Electr. Insul.* **23**, 43 (2016).
- ⁵⁰C. Chen, Y. C. Xie, M. R. Zhang, J. Li, X. Y. Wei and Z. C. Zhang, Significantly enhanced energy storage properties in sandwich-structured polymer composites with self-assembled boron nitride layers, *Appl. Surf. Sci.* **598**, 153673 (2022).